Topological analysis of group fragmentation in multiagent systems

Pietro DeLellis, Maurizio Porfiri, and Erik M. Bollt

Phys. Rev. E **87**, 022818 — Published 25 February 2013

DOI: 10.1103/PhysRevE.87.022818

Topological analysis of group fragmentation in multi-agent systems

Pietro DeLellis*
Department of Systems and Computer Engineering, University of Naples Federico II, Via Claudio 21, 80125, Naples, Italy.†

Maurizio Porfiri‡
Department of Mechanical and Aerospace Engineering, Polytechnic Institute of New York University, Brooklyn, NY 11201, USA.§

Erik M. Bollt¶
Department of Mathematics and Computer Science, Clarkson University, Potsdam, NY 13699-5815, USA.

In social animals, the presence of conflicts of interest or multiple leaders can promote the emergence of two or more subgroups. Such subgroups are easily recognizable by human observers, yet, a quantitative and objective measure of group fragmentation is currently lacking. In this paper, we explore the feasibility of detecting group fragmentation by embedding the raw data from the individuals' motions on a low-dimensional manifold and analyzing the topological features of this manifold. To perform the embedding, we employ the ISOMAP algorithm, which is a data-driven machine learning tool extensively used in computer vision. We implement this procedure on a data set generated by a modified à la Vicsek model, where agents are partitioned in two or more subsets and an independent leader is assigned to each subset. The dimensionality of the embedding manifold is shown to be a measure of the number of the emerging subgroups in the selected observation window and a cluster analysis is proposed to aid the interpretation of these findings. To explore the feasibility of using this approach to characterize group fragmentation in real time and thus reduce the computational cost in data processing and storage, we propose an interpolation method based on an inverse mapping from the embedding space to the original space. The effectiveness of the interpolation technique is illustrated on a testbed example with potential impact on the regulation of collective behavior of animal groups using robotic stimuli.

PACS numbers: 89.75.Fb, 02.70.-c, 05.65.+b, 87.23.Cc

I. INTRODUCTION

The coordinated motion of fish schools [1, 2], flocks of birds [3, 4], and swarms of insects or bacteria [5, 6] are all examples of collective behaviors in social animals. Elucidating the mechanisms that underlie such coordinated movements is the subject of considerable ongoing research [7–11]. Generally, collective behavior is associated to the formation of a sole self-organized group in which all members behave like an egalitarian "superorganism" [12]. However, a number of observations demonstrate the coexistence of a landscape of ordered subgroups characterized by different objectives and possible conflicts of interest [13–15]. The existence of such group partitions and their behavior can be readily distinguished by a human observer, yet a quantitative method for their characterization from raw data is to be established.

Beyond individual variations, the fragmentation of the group into smaller subgroups may also be elicited by the presence of multiple leaders differentially affecting the response of conspecifics [15–18] or even the presence of robotic stimuli administered to regulate the collective response of social animals [19–25]. In these latter applications, an open problem is to device control strategies for robots to take decision in real time based on the animals' collective response without either tracking the motion of each individual, or inferring their response from an underlying mathematical model.

Here, we provide a data-driven dynamical systems framework for characterizing group fragmentation in social animals based on methods from machine learning and computer vision. While numerical simulations have played a defining role in modeling and understanding collective behavior of multi-agent systems [3, 4, 26–30], these analyses generally rely on global observables that are defined on the basis of a priori knowledge of group behavior and often require explicit tracking of each agent. In the proposed framework, we seek to characterize collective behavior from raw video data, while minimizing the input from the experimenter in the data classification. This work builds on the recent findings presented in [31], wherein it is demonstrated that the formation of a unique group in the system corresponds to the existence of a nearly one-dimensional manifold embedding the raw

* pietro.delellis@unina.it
† Also at the Department of Mechanical and Aerospace Engineering, Polytechnic Institute of New York University, Brooklyn, NY 11201, USA.
‡ mporfiri@poly.edu
§ Author to whom all correspondence should be addressed.
¶ bolltem@clarkson.edu

data of individuals' motion. Computer simulations of a system of particles interacting in a modified à la Vicsek model [27] and experimental data of fish schooling are analyzed therein through the ISOMAP algorithm to extract the sought low-dimensional structures. The ISOMAP algorithm is an easy to implement dimensionality reduction method, which finds applications in computer vision and machine learning [32–34]. Differently than [31], here we focus on the emergence of multiple coexisting subgroups and we seek to establish a toolbox of analytical tools to transition the approach to practical scenarios wherein available data is limited in quality and size.

As a reference model for our analysis, we consider a system of agents with à la Vicsek interaction rules [27], wherein agents' grouping is manifested by individuals sharing common headings. Such framework is extensively studied in the literature [30, 35–39] and finds application in modeling schools of fish, correlated motion of pedestrians, flocks of flying birds, and bacterial colony growth [4, 17, 40–43]. Differently from the original Vicsek model, but preserving the same interaction rules, we allow for the presence of heterogeneous agent subsets that do not interact with each other. This feature, together with the presence of multiple leaders, is responsible for the formation of coexistent subgroups in the system against inherent noise in the individual dynamics. We show how the dimensionality of the embedding manifold detected by the ISOMAP algorithm can be considered as a measure of the number of subgroups in the system for the selected observation window. Specifically, in the presence of low noise, agents' headings cluster along the leaders' headings and we validate the hypothesis that the manifold dimensionality equals the number of leaders in the system through the analysis of the polarization [27] of each agents' subset. As noise in the system is increased, the ISOMAP algorithm produces embedding manifolds of increasing dimensionality which corresponds to the formation of ephemeral subgroups in the system. The formation of such subgroups is further detected by the kmeans clustering algorithm [44], which allows for a further classification of the dynamics taking place in the system.

Motivated by potential application to the robotic modulation of collective behavior, for which minimizing the size of the data set is of practical relevance, we propose an interpolation method based on an inverse mapping from the embedding manifold to the original space. The mapping uses linear combination of translates of a radial basis function [45]. We demonstrate the effectiveness of this approach on a testbed engineering example, where the system is partitioned into two subsets and one of the leaders is controlled to minimize fragmentation, that is, to merge the agents into a sole group. The developed interpolation method is shown to be effective in correctly detecting the variation in the system fragmentation from the analysis of a small data set acquired by the controlled leader.

The outline of the paper is as follows. In Section II, the interaction model for the multi-agent systems is described. In Section III, the ISOMAP algorithm is introduced and shown to be an effective tool for subgroups' detection. In Section IV, an inverse mapping is presented and the analysis is extended to the case of small data sets. Conclusions are drawn in Section V.

II. MODEL OF THE MULTI-AGENT SYSTEM

We consider a system of interacting agents moving in a two-dimensional domain with a constant speed s. The domain is a square of side length $L \in \mathbb{R}^+$ and we select periodic boundary conditions. We assume that agents are partitioned into M leaders and N followers, with agents $1, \dots, M$ being the leaders. Followers are further partitioned into M disjoint subsets $\mathcal{D}_1, \dots, \mathcal{D}_M$, with agents in the j-th subset being assigned to the j-th leader. The position of the i-th agent at time $k \in \mathbb{Z}^+$ is given by $x_i(k) \in \mathbb{C}$, whose real and imaginary part belong to $[-L/2, L/2]$ for $i = 1, \dots, N + M$. The heading of the i-th agent at time k is denoted by $\theta_i(k)$ and belongs to $[-\pi, \pi]$. The initial position and heading of the agents are both taken randomly from a uniform distribution.

The j-th leader moves with a preferential heading ϑ_j, for $j = 1, \dots, M$, and only influences the dynamics of the agents in subset $\mathcal{D}_j$, for $j = 1, \dots, M$. Followers update their headings according to the interactions with their neighbors. Such neighbors include other followers from the same subset within a distance $r \in \mathbb{R}^+$, that is, $\mathcal{N}_i^j(k) = \{c \in \mathcal{D}_j : \|x_c(k) - x_i(k)\| \leq r\}$, and the corresponding leader if it is within a distance $r_l \in \mathbb{R}^+$. Specifically, if the follower $i \in \mathcal{D}_j$ is far from its leader, then its heading at time step $k+1$ is computed by averaging its heading with the headings of the neighbors at time step k. Namely, we have

$$\theta_i(k+1) = \arg\left(\sum_{c \in \{i\} \cup \mathcal{N}_i^j(k)} e^{\imath \theta_c(k)} \right) + \Delta\theta,$$

where $\Delta\theta$ is a uniformly-distributed random variable which takes values in $[-\eta\pi, \eta\pi]$ with $\eta \in [0, 1]$ and $\imath$ is the imaginary unit. Otherwise, if the corresponding leader is within the distance r_l, then the averaging process also involves the leader and the corresponding heading $\theta_j(k)$ is weighted by ω. This process is used to model the influence of each leader on its followers, that is,

$$\theta_i(k+1) = \arg\left(\sum_{c \in \{i\} \cup \mathcal{N}_i^j(k)} e^{\imath \theta_c(k)} + \omega e^{\imath \theta_j(k)} \right) + \Delta\theta.$$

In summary, these two cases can be consolidated in the

following update rule

$$\theta_i(k+1) = \arg\left(\sum_{c\in\{i\}\cup\mathcal{N}_i^j(k)} e^{\imath\theta_c(k)} + \omega \underset{\mathcal{L}_j(k)}{\text{ind}}(i) e^{\imath\theta_j(k)} \right) + \Delta\theta, \quad (1)$$

where $\underset{\mathcal{L}_j(k)}{\text{ind}}(\cdot)$ is the indicator function for the neighbors of the j-th leader, and $\mathcal{L}_j(k) = \{c \in \mathcal{D}_j : \|x_c(k) - x_j(k)\| \leq r_l\}$. The heading of the leaders, instead, is not affected by the heading of the neighbors. Namely,

$$\theta_i(k+1) = \vartheta_i + \Delta\theta, \qquad i = 1, \ldots, M. \quad (2)$$

The position of all agents is updated according to

$$x_i(k+1) = x_i(k) + s e^{\imath\theta_i(k+1)}, \qquad i = 1, \ldots, N+M. \quad (3)$$

We comment that while the proposed approach is specialized to model (1), the analysis can be adapted to alternative models for multi-agent systems [22, 46–48].

III. SUBGROUPS' DETECTION THROUGH ISOMAP

In this section, after a brief review of the ISOMAP algorithm, we illustrate its effectiveness in detecting the presence of subgroups in the system.

A. ISOMAP algorithm

The ISOMAP algorithm is a method for computing a quasi-isometric low-dimensional embedding of a set of high-dimensional data points [32]. Here, we briefly review the main steps of the algorithm. We consider an array of n d-dimensional data points with the goal of embedding them on a possibly lower dimensional manifold. Namely, given a data set $\mathcal{Z} = \{z_i\}_{i=1}^n \subset \mathbb{R}^d$, we aim at building a corresponding data set $\mathcal{Y} = \{y_i\}_{i=1}^n \subset \mathbb{R}^{\bar{d}}$, embedded in an invariant manifold, and assessing if $\bar{d} \ll d$. The manifold can be represented through the following implicit parametrization

$$\mu : \mathcal{Y} \to \mathcal{Z}, \quad (4)$$

where

$$z_{ij} = \mu_j(y_{i1}, \ldots, y_{i\bar{d}}), \quad (5)$$

for $i = 1, \ldots, n$, and $j = 1, \ldots, d$. Here, the second subscript is used to identify vector components.

The ISOMAP algorithm is based on the classical multidimensional scaling method (MDS) [49], which is not applied to the ambient Euclidean space, but rather considers shortest paths along a discrete graph approximation of the manifold. The main steps of the algorithm can be summarized as follows:

1. **Construct a neighbors graph to approximate the embedding manifold**. We introduce the graph $\mathcal{G} = \{\mathcal{V}, \mathcal{E}\}$: the elements of the set of vertices $\mathcal{V} = \{v_i\}_{i=1}^n$ match the data points $\mathcal{Z} = \{z_i\}_{i=1}^n$, while the elements of the set of edges $\mathcal{E}$ are unordered pairs of vertices in the graph. We assign edges to connect vertices that are either ϵ-neighbors or ν-nearest neighbors. For instance, we can build a ν-nearest neighbors graph, consisting of edges $\{v_i, v_j\}$ corresponding to the ν-closest data points z_j to z_i, for each $i = 1, \ldots, n$, with respect to the Euclidean distance in the ambient space, denoted by $d_Z(z_i, z_j)$. We define $M_n \in \mathbb{R}^{n\times n}$ as the matrix encoding the weighted graph of intrinsic manifold distances corresponding to the graph $\mathcal{G}$, whose ij-th entry is denoted by $M_n(i, j)$. For each edge $\{v_i, v_j\} \in \mathcal{E}$, we define the distances $M_n(i, j) \approx d_Z(z_i, z_j)$ and for all $\{v_i, v_j\} \notin \mathcal{E}$, we set $M_n(i, j) = \infty$ to prevent jumps between branches of the underlying manifold.

2. **Compute the graph geodesic matrix approximating the geodesic of the manifold**. This step can be performed using well-established methods to compute shortest paths, such as Floyd's algorithm [50] for small to medium sized data sets or Dijkstra's algorithms [51] for small to large data sets. From M_n, we compute an approximate geodesic distance matrix $D_M \in \mathbb{R}^{n\times n}$, whose ij-th element is the shortest weighted path length between each v_i to v_j, being an approximation of manifold geodesic distances.

3. **Approximate manifold distance by ν-nearest neighbor distance**. The distance matrix D_M from step 2) approximates the geodesic distances of the manifold between z_i and z_j by the distance between v_i and v_j. The accuracy of the approximation increases with data density. If ν is too large or data density is too low, then some neighbors could be on separate branches of the manifold, resulting in a poor representation of the manifold.

4. **Perform an MDS on D_M**. The only input to the MDS is D_M, that is computed in step 2) from the input data $\mathcal{Z}$. The outputs are the projective variables $\mathcal{Y}$ in the intrinsic variables.

The outputs of the ISOMAP algorithm are an embedding manifold for the input data set $\mathcal{Z}$ and the vector R of residual variances, which, in turn, quantifies the proportion of data points not lying on such manifold. From the norm of the residual variances, we determine the dimensionality of the embedding manifold that well approximates $\mathcal{Z}$. If this overall residual variance for dimension one is less than 0.05, we say that the embedding manifold has dimension one. If this is not the case, we seek for an elbow in this curve. As a quantitative definition of the elbow location, we select a decrease of the

residual variance, scaled with respect to dimension one, to less than 0.05.

B. Subgroups' detection

In [31], it is shown that the ISOMAP algorithm is effective in detecting the presence of collective behavior of animal groups acting as a single superorganism. Here, we show how ISOMAP can be used for gathering additional information on the nature of the system dynamics and, particularly, to learn about group fragmentation. To illustrate our claims, we consider three different scenarios for model (1), wherein the system is composed of one, two, or three subsets.

In the following simulations, we acquire the two-dimensional positions of the agents and implement the ISOMAP algorithm on their distribution in a discretized spatial domain: the original domain $[-L/2, L/2] \times [-L/2, L/2]$ is partitioned into a square two-dimensional grid of 50×50 cells, that can be viewed as "pixels of an image on a screen". At every time step, the entries of the 1×2500 position distribution vector report the number of agents residing in each cell.

Here, we consider $N = 40$ followers and we take $L = 50$, $s = 0.12$, $r = 1$, $r_l = 2$, $\eta = 0.005$, and $\omega = 40$. The length of each simulation is of $k_{\max} = 20000$ time steps, while the ISOMAP algorithm is performed on the last $n = 2000$ data points ordered in time. With reference to the steps in Section III.A, we execute step 1) with 11-nearest neighbors and we use Dijkstras algorithm for performing step 2). For simulations with a single leader, its preferential heading is $\pi/6$. For the case of two leaders, we take $\vartheta_1 = \pi/6$ and $\vartheta_2 = \pi/3$. For three leaders, we set $\vartheta_1 = \pi/6$, $\vartheta_2 = \pi/3$, and $\vartheta_3 = 4\pi/3$.

As an independent measure of grouping in the multi-agent system, we introduce the polarization of the m-th followers' subset with the corresponding leader:

$$\mathrm{Pol}_m(k) = \frac{1}{|\mathcal{D}_m| + 1} \left\| \sum_{i \in \mathcal{D}_m} e^{\imath\theta_i(k)} + e^{\imath\theta_m(k)} \right\| \qquad (6)$$

where $m = 1, \ldots, M$. This quantity ranges from 0 to 1 and is equal to 1 if followers in that subset share the same heading of their leader. Notably, in the limit of a large number of agents, the polarization is used to detect phase transitions [27]. Additional global observables to describe collective behavior can be found in [24, 52].

When the system is homogeneous, that is, the followers' set is not partitioned into subsets, Figure 1(d) demonstrates that the dimension of the manifold is one in agreement with [31]. In this case, all the agents in the system move with a common heading as evidenced by the time trace of the polarization in Figure 2(a). In the presence of two leaders, the two followers' subsets are $\mathcal{D}_1 = \{1, \ldots, 20\}$ and $\mathcal{D}_2 = \{21, \ldots, 40\}$ and the manifold appears to be sharply two-dimensional, as illustrated in Figures 1(b) and 1(e). In this case, each followers' subset tracks its leader as illustrated in Figure 2(b). In the case of three leaders, the followers' partition is $\mathcal{D}_1 = \{1, \ldots, 13\}$, $\mathcal{D}_2 = \{14, \ldots, 26\}$, and $\mathcal{D}_3 = \{27, \ldots, 40\}$. For this system, the proposed methodology indicates the existence of a three-dimensional manifold corresponding to three subgroups, see Figure 1(f). Such structure corresponds to each follower tracking its corresponding leader, as depicted in Figure 2(c). We comment that, whereas a differentiable manifold is characterized by the presence of a well-defined tangent space at each point, dynamical systems can give rise to attractors embedded in branched manifolds [53]. The latter generalize the notion of differentiable manifolds in that certain points may have singularities. In the case of multi-agent systems that fragment into distinct subgroups, it could be expected a priori that a branched manifold may result and, indeed, Figures 1(e) and 1(f) suggest this scenario. Nonetheless, for the sake of local modeling, most points are still well described by a tangent space. Similar practices have been used in the parallel problem of nonlinear time series prediction [54–56].

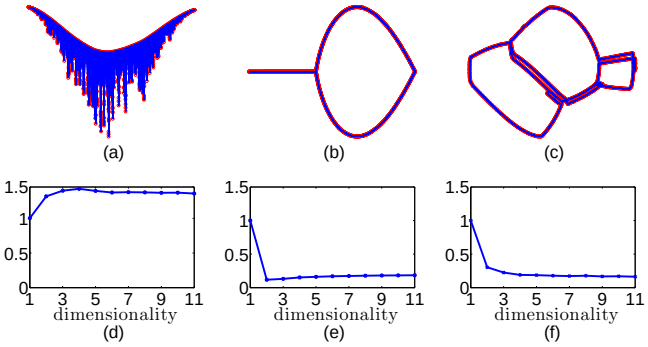

FIG. 1. (Color online) Two-dimensional embedding manifolds generated by the ISOMAP algorithm (top) and scaled residual variance (bottom) for one (left), two (center), and three (right) leaders and $\eta = 0.005$. Residual variances for dimension one are: 2.20×10^{-5}, 0.24, 0.34 for 1, 2, and 3 subsets, respectively.

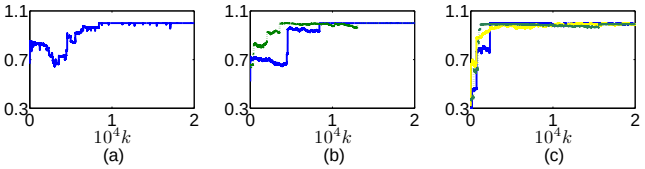

FIG. 2. (Color online) Time trace of the polarization for varying number of leaders and $\eta = 0.005$.

These findings demonstrate a close correspondence between subgroups' detection using the proposed data-driven dynamical system framework and supervised analysis based on ad hoc global observables when the noise in the system is limited. Figure 3(b) illustrates findings for the case of two leaders, earlier considered in Figures 1(b) and 1(e), when the noise is raised to $\eta = 0.025$. Figure 3(b) shows that, as the noise increases, the ISOMAP al-

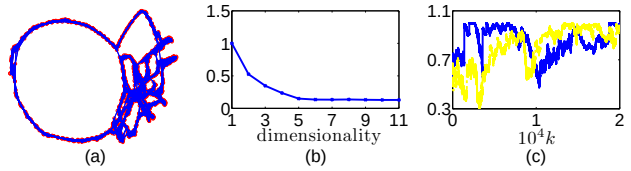

FIG. 3. (Color online) Results for simulations involving two agents' subsets with $\eta = 0.025$: two-dimensional embedding manifolds generated by the ISOMAP algorithm (left); scaled residual variance (center); and time trace of the polarization (right). Residual variance for dimension one is 0.26.

gorithm detects the formation of a larger number of subgroups. Indeed, as the noise increases, the elbow in the residual curve slowly shifts towards larger dimensions. At the same time, the average polarization of each subset rapidly decreases while displaying larger oscillations in time. Such oscillations indicate the recurrence of ordered states within each subsystem which cyclically arise and disappear in time [57] and are thus filtered by the ISOMAP algorithm which operates on the last 2000 time steps. Thus, the modest increase in the embedding manifold dimensionality is likely to be due to the interplay of two factors: the presence of two agents' subsets with different leaders' heading and the oscillations inside each partition due to the presence of noise, which may be responsible of complex landscapes of headings' clustering [57].

To shed further light on the system dynamics while avoiding the tracking of each agent trajectory, we complement ISOMAP with a cluster analysis executed on the two-dimensional coordinates $\{q_i\}_{i=1}^{Q(k)} \in \mathbb{R}^2$ of the pixels identifying the agents on the screen, referred to as "activated pixels" for brevity, where $Q(k)$ is the total number of pixels occupied by the agents at time k. In particular, we seek to infer the process of fragmentation and aggregation within the multi-agent system by analyzing the time trace of the number of clusters $\upsilon^*(k)$ for the activated pixels. The implementation is performed by using the so-called silhouette index [58] while assuming that $\upsilon^*(k)$ is considerably smaller than the number of agents in the system, that is, $\upsilon^*(k) < c \ll N + M$. To this aim, the following steps are performed at each time instant k:

1. **Execute the kmeans algorithm $c-1$ times and analyze intra/inter-cluster distances.** For each tentative number of clusters $\upsilon = 2, \ldots, c$, we implement the kmeans algorithm [44] to partition the set $\{q_i\}_{i=1}^{Q(k)}$ into υ disjoint subsets with indices in the clusters $\mathcal{C}_1(k), \ldots, \mathcal{C}_\upsilon(k)$. Once these clusters are assembled, for $j = 1, \ldots, \upsilon$ we calculate the average intra-cluster distance between each activated pixel $i \in \mathcal{C}_j$ and the other activated pixels in the same cluster. Namely, we compute

$$a_i^j(k) = \frac{1}{|\mathcal{C}_j(k)| - 1} \sum_{\substack{l \in \mathcal{C}_j(k) \\ l \neq i}} \|q_i(k) - q_l(k)\|,$$

for $j = 1, \ldots, \upsilon$ and $i \in \mathcal{C}_j(k)$. In addition, we compute the minimum average inter-cluster distance between each activated pixel $i \in \mathcal{C}_j$ and the activated pixels in any other cluster $\mathcal{C}_h$, with $h \neq j$. Specifically, we calculate

$$b_i^j(k) = \min_{h \neq j} \left\{ \frac{1}{|\mathcal{C}_h(k)|} \sum_{l \in \mathcal{C}_h(k)} \|q_i(k) - q_l(k)\| \right\},$$

for $j = 1, \ldots, \upsilon$ and $i \in \mathcal{C}_j(k)$.

2. **Compute the silhouette width of each activated pixel for all clustering trials.** For $\upsilon = 2, \ldots, c$, we calculate the silhouette width of pixel i in cluster $\mathcal{C}_j(k)$ as

$$S_i^j(k, \upsilon) = \frac{b_i^j(k) - a_i^j(k)}{\max\{a_i^j(k), b_i^j(k)\}},$$

for $j = 1, \ldots, \upsilon$ and $i \in \mathcal{C}_j(k)$. The silhouette width of an activated ranges from -1 to 1. Values proximal to 1 indicate that the average intra-cluster distance of the activated pixel is much higher than any of its average inter-cluster distances. On the other hand, values close to -1 indicate that, for some cluster $\mathcal{C}_h(k)$, with $h \neq j$, the corresponding average inter-cluster distance of the activated pixel i is much higher than its average intra-cluster distance.

3. **Determine the optimal number of clusters.** The sought number of clusters $\upsilon^*(k)$ is determined by solving an optimization problem for the mean silhouette index as a function of υ, defined as

$$S_{\text{av}}(k, \upsilon) = \frac{1}{\upsilon\, |\mathcal{C}_j(k)|} \sum_{j=1}^{\upsilon} \sum_{i \in \mathcal{C}_j(k)} S_j^i(k, \upsilon).$$

Specifically, we solve

$$\upsilon^*(k) = \underset{\upsilon = 2, \ldots, c}{\text{argmax}}\, S_{\text{av}}(k, \upsilon). \tag{7}$$

In practice, when the dimension of the embedding manifold is larger than one, we propose to use a cluster analysis to garner a further understanding of the system dynamics without tracking individuals' trajectories. We compute the number of clusters $\upsilon^*(k)$ in the same time window considered for the ISOMAP and then we analyze the statistical properties of its distribution to identify the emergence of either temporally-stable or ephemeral subgroups in the system. Figures 4(a) and 4(b) illustrate results from the cluster analysis implemented on the multi-agent system in presence of two leaders for the varying noise levels considered in Figures 1(b) and 1(e) and Figures 3(a) and 3(b), respectively.

As depicted in Figures 4(a), for low noise in the system, the number of clusters is two for almost all times. This peaked distribution confirms the consistent fragmentation of the system in two subgroups. As the noise in

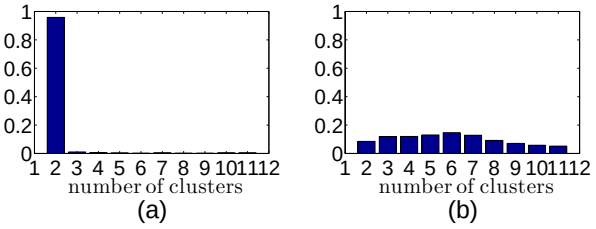

FIG. 4. (Color online) Comparison of the distribution of the number of clusters for simulations in presence of two agents' subsets: $\eta = 0.005$ (left) and $\eta = 0.025$ (right).

the system increases, the dynamics of fragmentation is significantly different. In this case, the probability that the group is organized in two subgroups is much smaller, about the 8%, while the effect of the noise is to split the system into three or more subgroups, with the mode of the distribution being equal to six. Hence, the higher dimensionality identified by the ISOMAP algorithm, see Figure 3(b), is well explained by the continuous fragmentation and aggregation of the agents. We comment that the analysis is unlikely to offer valuable insight on the formation and disintegration of subgroups, for the Vicsek model, in case that the interaction radius r is comparable with the domain length L. In this case, agents would be able to group along certain headings without spatially splitting into observable clusters as those detected through the mean silhouette index.

IV. ANALYSIS OF SMALL DATA SET

The ISOMAP algorithm, possibly complemented by a cluster analysis, can be effectively used for subgroups' detection without the need for tracking the individual agents' dynamics. In view of possible control applications, it is crucial to understand the requirements on the size of the data set to allow for a proper identification of its fragmentation through the ISOMAP algorithm and establish methodologies for a-posteriori increasing the data density.

A. Interpolation through inverse mapping

When the data set under analysis is small, the dimensionality detected by the ISOMAP algorithm may be misleading, as further illustrated in simulations presented below. Hence, we propose to enrich the data set by: i) performing a standard interpolation of the data embedded on the low-dimensional manifold to add new points therein and ii) mapping the newly added points back to the original space.

The first step can be executed by using linear interpolation, that is, by connecting adjacent data points on the manifold, say y_k and y_{k+1}, with $k = 1, \dots, n-1$ through an interpolating hyperplane. Once such hyperplanes are constructed for all times, points are added to the manifold by sampling along the hyperplanes with a prescribed refinement ρ, so that ρ values are added between y_k and y_{k+1}, with $k = 1, \dots, n-1$.

The second step requires the construction of an inverse mapping. We aim at approximating the maps $\mu_1, \dots, \mu_d$ in (5) through d mappings

$$\hat{\mu}_j : \mathbb{R}^{\bar{d}} \to \mathbb{R}, \qquad j = 1, \dots, d, \tag{8}$$

such that

$$z_{ij} = \hat{\mu}_j(y_{i1}, \dots, y_{i\bar{d}}), \qquad i = 1, \dots, n,\ j = 1, \dots, d. \tag{9}$$

The approximation is performed using linear combinations of translates of a rotationally invariant function, called radial basis function [45]. Approximation through radial basis functions is a well-established approach in the field of learning theory with excellent convergence properties [59] along with fast computational implementation [60]. In our interpolation, we consider the multiquadratic function $\varphi(u, \alpha) = \sqrt{u^2 + \alpha^2}$, with $\alpha \in \mathbb{R}$, which is a conditionally positive definite radial function of order one [61]. In this context, the approximating function is given by

$$\hat{\mu}_j(\xi, \alpha) = \sum_{i=1}^{\bar{n}} w_{ij}(\alpha) \varphi\left(\|\xi - \beta_i\|, \alpha\right), \tag{10}$$

for $\xi \in \mathbb{R}^{\bar{d}}$, where w_{ij} are coefficients to be estimated and $\bar{n} \leq n$ is the number of reference points $\beta_1, \dots, \beta_{\bar{n}} \in \mathbb{R}^{\bar{d}}$ used for the interpolation. Such points are generally different from the original data points $y_1, \dots, y_n$.

Equations (9) and (10) can be rewritten in matrix form as

$$\Phi(\alpha) W(\alpha) = Z, \tag{11}$$

where $\Phi(\alpha) \in \mathbb{R}^{n \times \bar{n}}$ with $\Phi_{ij}(\alpha) = \varphi\left(\|y_i - \beta_j\|, \alpha\right)$, $Z = [z_1 \cdots z_n]^T \in \mathbb{R}^{n \times d}$, and $W(\alpha) \in \mathbb{R}^{\bar{n} \times d}$ is the coefficient matrix to be estimated. For a selection of the parameter α, the matrix of coefficients W can be calculated from the pseudoinverse of $\Phi(\alpha)$ [62]. Once the matrix $W(\alpha)$ is computed, all the coefficients in (10) are available along with the approximating maps (9) which can be used to calculate new points in the original space from the refined points on the manifold. We refer to the data set composed of $y_1, \dots, y_n$ and these newly added data points as the "synthetic" data set. Estimating the local manifold based on fitting hyperplanes to the nearby observations has a strong background in dynamical systems theory and specifically in the extensive literature on time-delay embedding prediction [54–56].

B. Subgroups' detection in a control example

Here, we analyze the effectiveness of the approximation technique described above on a testbed control example.

By control we mean that the followers are divided in two subsets $\mathcal{D}_1$ and $\mathcal{D}_2$ and the leader of $\mathcal{D}_1$ is controlled to align the heading of its followers with $\mathcal{D}_2$. We assume that the controlled leader acquires the discretized data from video recordings and is thus not able to track individually the trajectory of the agents. Yet, we hypothesize that agents belonging to the two subsets can be distinguished for control purposes. To model practical limitations in the experimental design, we assume that the controlled leader possesses finite memory and only 500 frames can be stored and processed. In what follows, we first describe the control algorithm and then analyze the system fragmentation through the ISOMAP algorithm when the only available data are those currently stored by the controlled leader.

In this control example, we consider the same parameters as in Section III, except for the simulation time which is doubled, that is, $k_{\max} = 40000$. The preferential heading of the leader of $\mathcal{D}_2$ is $\vartheta_2 = 2\pi/3$, the initial heading of the controlled leader is $\vartheta_1(0) = \pi/3$, and $\eta = 0.005$. The preferential heading of the controlled leader is held to $\vartheta_1(0)$ until the control system is triggered. The controlled leader stores frames every 4 time steps and executes the cluster analysis in Section III on them. The control algorithm is triggered at the first time instant when the controlled leader observes the presence of two stable clusters. For the selected initial conditions, the control system is activated at time $k_0 = 20100$ when the leader identifies the presence of two clusters over 80% of its observations. For $k \geq k_0$, the controlled leader updates its heading according to

$$\theta_1(k+1) = \vartheta_1(k) + \Delta\theta,$$
$$\vartheta_1(k+1) = \vartheta_1(k) + u(k),$$

where $u(k)$ is the control input. To select the input $u(k)$, the controlled leader initially estimates the heading of the agents in the other subset. To this aim, it estimates the position of the center of mass of the uncontrolled agent subset in the last two stored frames from the coordinates of the activated points at time steps $k-4$ and k, respectively. Then, the average heading of the agents in the uncontrolled subset at time k is estimated as

$$\hat{\theta}_2(k) = \arg\left(\hat{x}_{\rm cm}(k) - \hat{x}_{\rm cm}(k-4)\right),$$

where $\hat{x}_{\rm cm}(k)$ is the estimated location of the center of mass of the uncontrolled agent subset. The control input is selected so that the preferential heading of the controlled leader is the average of $\hat{\theta}_2$ over the last stored 500 frames. Namely,

$$\bar{u}(k) = \frac{1}{500}\sum_{i=0}^{499} \hat{\theta}_2(k-4i) - \vartheta_1(k).$$

Figure 5(a) demonstrates that the controlled leader is able to accurately track the heading of the other leader as soon as the control system is activated. The effectiveness of the algorithm can be evaluated by computing the polarization for the whole system

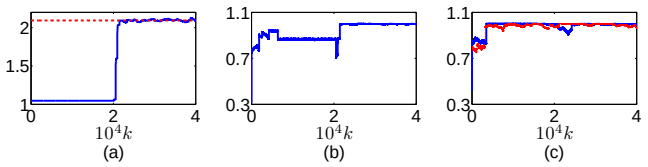

FIG. 5. (Color online) Assessment of the control algorithm performance: headings of leader 1 (blue solid line) and 2 (red dashed line) in radians (left); time trace of the polarization of the whole system (center); time trace of the polarization for subset 1 (blue solid line) and subset 2 (red dashed line) (right).

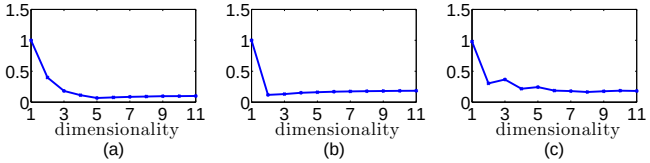

FIG. 6. (Color online) Scaled residual variance for the ISOMAP algorithm for the time windows [1 2000] (left), [18001 20000] (center), [38001 40000] (right) of the control example implemented on all the available 2000 samples. Residual variances for dimension one are: 0.38, 0.23, 0.01 for time windows [1 2000], [18001 20000], and [38001 40000], respectively.

$$\mathrm{Pol}(k) = \frac{1}{N+M}\left\|\sum_{i=1}^{N+M} e^{\imath\theta_i(k)}\right\|.$$

This index is designed so that it equals one when all agents in the system [27], followers and leaders, have the same heading, that is, when the control objective is attained. Figure 5(b) shows that at the onset of the simulation the multi-agent system is in a highly disorganized state and eventually behaves as a single group when the control system is triggered. Notably, when the control system is activated, two subgroups are present in the system, corresponding to followers tracking the heading of the corresponding leader, see Figure 5(c). In other words, joining a single group entails forming two sub-

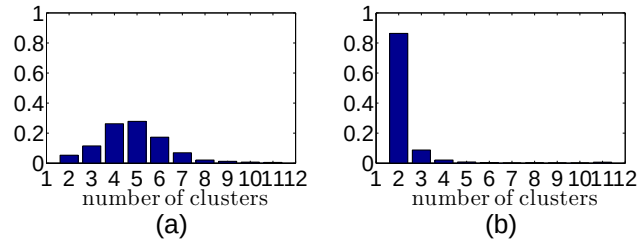

FIG. 7. (Color online) Distribution of the number of clusters for the control example computed over: the time windows [1 2000] (left) and the time window [18001 20000] (right).

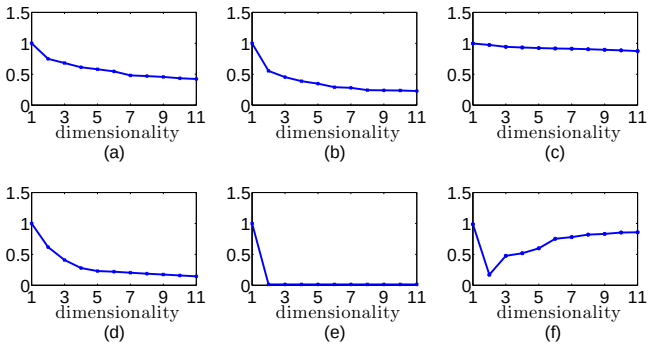

FIG. 8. (Color online) Scaled residual variance for the ISOMAP algorithm executed on varying time windows of the control example and based on 500 samples obtained through uniform downsampling. Results in top panels are implemented on a data set of only 500 samples, while findings in bottom panels use 2000 synthetic samples obtained from the 500 uniformly downsampled data points. For top panels, the time windows are: [1 2000] (left), [18001 20000] (center), and [38001 40000] (right) with residual variances for dimension one equal to 0.92, 0.61, and 0.99, respectively. For bottom panels, the time windows are: [1 2000] (left), [18001 20000] (center), and [38001 40000] (right) with residual variances for dimension one equal to 0.45, 0.34, and 0.01, respectively.

groups which are then merged as the control system is activated.

To dissect the system dynamics during the whole simulation time, we execute the ISOMAP algorithm on the three representative time windows [1 2000], [18001 20000], and [3800140000]. Figure 6(a) demonstrates that the proposed approach is able to identify the process of grouping taking place in the multi-agent system through a dimensionality of the embedding manifold equal to five. The algorithm is also able to detect the formation of two temporally-stable subgroups prior to the activation of the control system through an embedding manifold of dimensionality equal to two, see Figure 6(b). The cluster analysis presented in Figures 7(a) and 7(b) further illustrates the fundamental differences between the state of the multi-agent system in these two time windows. While a broad variation of the number of clusters is observed at the onset of the simulation, two stable clusters develop before the control activation. Finally, the emergence of a single group corresponding to the accomplishment of the control objective is manifested through the detection of an embedding manifold of dimension equal to one, see Figure 6(c).

If the ISOMAP algorithm were performed only on the 500 frames stored by the controlled leader, the identification of subgroups in the system would fail. Indeed, embedding manifolds stemming from the analysis of such downsampled data have dimensions which are consistently higher than the number of subgroups identified from the whole data set, see Figures 8(a), 8(b) and 8(c). Yet, the data stored by the controlled leader is sufficient for characterizing the formation of subgroups in the system, as demonstrated in Figures 8(d), 8(e) and 8(f), where the downsampled data set is enriched through the procedure explained in Section IV A. In other words, detection of subgroups in the system is also possible for smaller data sets provided that a larger synthetic data set is fed into the ISOMAP algorithm.

V. CONCLUSIONS

In this paper, we have presented a data-driven dynamical systems framework to study fragmentation in multi-agent systems. The approach uses raw data from the agents' motion to construct a low-dimensional manifold where collective behavior is manifested and whose dimensionality is a direct measure of the numbers of subgroups constituting the multi-agent system. The detection of such low-dimensional embedding manifold is executed through the ISOMAP algorithm, that is a well-established tool for dimensionality reduction in large data sets with extensive applications in computer vision.

The proposed methodology has been illustrated through the analysis of simulation data of a system of à la Vicsek self-propelled particles, where agents are partitioned into different subsets, each of them being guided by a separate leader. In this model, agents are bound to interact only with individuals from the same subset and, for limited noise in the model, the leaders produce the formation of well organized and temporally-stable subgroups. As the noise in the model is increased, these patterns in the agents' motion are lost in favor of ephemeral subgroups of varying size.

The ISOMAP algorithm has been shown to effectively detect the formation of subgroups in the simulated data set for limited noise in the system. Indeed, the embedding manifold constructed through such algorithm has dimension equal to the number of subgroups as confirmed by analyzing the polarization of each subset composing the multi-agent system. As the noise in the model is increased, the dimensionality of the embedding manifold becomes larger and a cluster analysis is proposed to investigate the determinants of such variation. Specifically, the kmeans algorithm is used to understand whether the increase of dimensionality of the embedding manifold is due to the agents steadily being subject to a stronger noise in their heading update or splitting in a larger number of subgroups.

The success of the proposed methodology depends on the size and density of the data set available to execute the ISOMAP algorithm. Indeed, when the data set are merely downsampled, the accuracy of subgroups' detection may be reduced with false interpretation of the fragmentation process. To mitigate this effect while allowing for performing the analysis with limited data storage capabilities, we have proposed a procedure to generate synthetic data set from downsampled motions of the multi-agent system. The approach uses an interpolation method based on an inverse mapping from the low-

dimensional manifold to the original ambient space.

The overall framework has been shown to be successful in characterizing the fragmentation of the multi-agent system in an ample spectrum of conditions. In particular, we have explored the feasibility of detecting the formation of subgroups under varying levels of noise in the decision process and number of coexistent leaders. Such leaders are either bound to move along prescribed directions or can vary their heading in real time based on selected control objectives. The latter implementation is amenable for informing the design of control systems and experimental methods for regulating the collective behavior of social animals using robotic stimuli.

ACKNOWLEDGMENTS

Pietro De Lellis and Maurizio Porfiri were supported by the National Science Foundation under grants nos. CMMI-1129820 and CMMI-0745753. Erik M. Bollt was supported by the National Science Foundation under grant no. CMMI-1129859 and the Army Research Office under grant no. 61386-EG.

[1] B. L. Partridge, Scientific American **246**, 114 (1982).
[2] I. Aoki, Bulletin of the Japanese Society of Scientific Fisheries **50**, 751 (1984).
[3] C. W. Reynolds, in *SIGGRAPH '87 Proceedings of the 14th annual conference on Computer graphics and interactive techniques* (1987).
[4] M. Ballerini, N. Cabibbo, R. Candelier, A. Cavagna, E. Cisbani, I. Giardina, V. Lecomte, A. Orlandi, G. Parisi, A. Procaccini, M. Viale, and V. Zdravkovic, Proceedings of the National Academy of Sciences **105**, 1232 (2008).
[5] H. P. Zhang, A. Be'er, R. S. Smith, E. Florin, and H. L. Swinney, Europhysics Letters **87**, 48011 (2009).
[6] N. R. Franks, S. C. Pratt, E. B. Mallon, N. F. Britton, and D. J. T. Sumpter, Philosophical Transactions of the Royal Society B **357**, 1567 (2002).
[7] S. Gueron, S. A. Levin, and D. I. Rubenstein, Journal of Theoretical Biology **182**, 85 (1996).
[8] D. Grünbaum, Evolutionary Ecology **12**, 503 (1998).
[9] S. G. Reebs, Animal Behaviour **59**, 403 (2000).
[10] J. K. Parrish, S. V. Viscido, and D. Grünbaum, Biological Bulletin **202**, 296 (2002).
[11] T. D. Seeley, Biological Bulletin **202**, 314 (2002).
[12] D. S. Wilson and E. Sober, Journal of Theoretical Biology **136**, 337 (1989).
[13] S. A. Rands, G. Cowlishaw, R. A. Pettifor, J. M. Rowcliffe, and R. A. Johnstone, Nature **423**, 432 (2003).
[14] M. E. Gompper, Behavioral Ecology **7**, 254 (1996).
[15] L. Conradt, J. Krause, I. D. Couzine, and T. J. Roper, The American Naturalist **173**, 304 (2009).
[16] T. J. Pitcher and J. K. Parrish, "The behaviour of teleost fishes," (Chapman and Hall, London, 1993) Chap. Functions of shoaling behaviour in teleosts, p. 363–440.
[17] I. D. Couzin, J. Krause, R. Franks, and S. A. Levin, Nature **433**, 513 (2005).
[18] I. D. Couzin, Trends in Cognitive Science **13**, 36 (2009).
[19] R. Vaughan, N. Sumpter, J. Henderson, and A. Frost, Robotics and Autonomous Systems **31**, 109 (2000).
[20] J. Halloy, G. Sempo, G. Caprari, C. Rivault, M. Asadpour, F. Tâche, I. Saïd, V. Durier, S. Canonge, J. M. Amé, C. Detrain, N. Correll, A. Martinoli, F. Mondada, R. Siegwart, and J. L. Deneubourg, Science **318**, 1155 (2007).
[21] J. J. Faria, J. R. G. Dyer, R. O. Clément, I. D. Couzin, N. Holt, A. J. W. Ward, D. Waters, and J. Krause, Behavioral Ecology and Sociobiology **64**, 1211 (2010).
[22] M. Aureli and M. Porfiri, Europhysics Letters **92**, 40004 (2010).
[23] M. T. Rashid, M. Frasca, A. A. Ali, R. S. Ali, L. Fortuna, and M. G. Xibilia, Nonlinear Dynamics **68**, 555 (2012).
[24] M. Aureli, F. Fiorilli, and M. Porfiri, Physica D **241**, 908 (2012).
[25] G. Polverino, N. Abaid, V. Kopman, S. Macri, and M. Porfiri, Bioinspiration & Biomimetics **7**, 036019 (2012).
[26] M. Granovetter, American Journal of Sociology **83**, 1420 (1978).
[27] T. Vicsek, A. Czirók, E. Ben-Jacob, I. Cohen, and O. Shochet, Physical Review Letters **75**, 1226 (1995).
[28] A. Czirók and T. Vicsek, Physica A **281**, 17 (2000).
[29] I. D. Couzin, J. Krause, R. James, G. D. Ruxton, and N. R. Franks, Journal of Theoretical Biology **218**, 1 (2002).
[30] H. Chaté, F. Ginelli, G. Grégoire, F.Peruani, and F. Raynaud, The European Physical Journal B **64**, 451 (2008).
[31] N. Abaid, E. Bollt, and M. Porfiri, Physical Review E **85**, 041907 (2012).
[32] J. B. Tenenbaum, V. de Silva, and J. C. Langford, Science **290**, 2319 (2000).
[33] M. Balasubramanian and E. L. Schwartz, Science **295**, 7 (2002).
[34] M.-H. Yang, in *Proceedings of the 2002 International Conference on Image Processing* (2002).
[35] A. Czirók, A. L. Barabási, and T. Vicsek, Physical Review Letters **82**, 209 (1999).
[36] A. Jadbabaie, J. Lin, and A. S. Morse, IEEE Transactions on Automatic Control **48**, 988 (2003).
[37] A. V. Savkin, IEEE Transactions on Automatic Control **49**, 981 (2004).
[38] G. Grégoire and H. Chaté, Physical Review Letters **92**, 025702 (2004).
[39] G. Baglietto and E. V. Albano, Physical Review E **80**, 050103(R) (2009).
[40] A. Czirók, E. Ben-Jacob, I. Cohen, and T. Vicsek, Physical Review E **54**, 1791 (1996).
[41] D. Helbing, J. Keltsch, and P. Molnár, Nature **388**, 47 (1997).
[42] N. Abaid and M. Porfiri, Journal of the Royal Society Interface **7**, 1441 (2010).
[43] T. Vicsek, Nature **483**, 411 (2012).
[44] J. A. Hartigan and M. A. Wong, Journal of the Royal Statistical Society. Series C (Applied Statistics) **28**, 100

(1979).
[45] J. Blackburn and E. Ribeiro, in *Proceedings of the 2nd conference on Human motion: understanding, modeling, capture and animation* (2007).
[46] W. Ebeling, F. Schweitzer, and B. Tilch, Biosystems **49**, 17 (1999).
[47] M. R. D'Orsogna, Y. L. Chuang, A. L. Bertozzi, and L. S. Chayes, Physical Review Letters **96**, 104302 (2006).
[48] D. E. O. Juanico, Europhysics Letters **86**, 48004 (2009).
[49] T. F. Cox and M. A. Cox, *Multidimensional scaling* (Chapman and Hall, London, 1994).
[50] R. W. Floyd, Communications of the ACM **48**, 345 (1962).
[51] E. W. Dijkstra, Numerische Mathematik **1**, 269 (1959).
[52] Y.-L. Chuang, M. R. D'Orsogna, D. Marthaler, A. L. Bertozzi, and L. S. Chayes, Physica D **232**, 33 (2007).
[53] R. F. Williams, Publications Mathématiques de L'IHÉS **43**, 169 (1974).
[54] J.-P. Eckmann and D. Ruelle, Reviews of modern physics **57**, 617 (1985).
[55] J. D. Farmer and J. J. Sidorowich, Physical Review Letters **59**, 845 (1987).
[56] E. M. Bollt, International Journal of Bifurcation and Chaos **10**, 1407 (2000).
[57] H. Chaté, F. Ginelli, G. Grégoire, and F. Raynaud, Physical Review E **77**, 046113 (2008).
[58] P. J. Rousseeuw, Journal of Computational and Applied Mathematics **20**, 53 (1987).
[59] M. D. Buhmann, *Radial basis functions: theory and implementations* (Cambridge University Press, Cambridge, 2003).
[60] R. K. Beatson and M. J. D. Powell, "Numerical analysis 1993," (Longman, Burnt Mill, 1994) Chap. An Iterative method for thin spline interpolations that employs approximation to Lagrange functions, pp. 17–39.
[61] C. A. Micchelli, Constructive Approximation **2**, 11 (1986).
[62] G. H. Golub and C. F. Van Loan, *Matrix computations* (The Johns Hopkins University Press, Baltimore, 1996).
[63] E. Ben-Jacob, O. Schochet, A. Tenenbaum, I. Cohen, A. Czirók, and T. Vicsek, Nature **368**, 46 (1994).